

# Unifying Perspective of the Ultrafast Photodynamics of Orange Carotenoid Proteins from *Synechocystis*: Peril of High-Power Excitation, Existence of Different $S^*$ States, and Influence of Tagging

Stanisław Niziński, Adjéle Wilson, Lucas M. Uriarte, Cyril Ruckebusch, Elena A. Andreeva, Ilme Schlichting, Jacques-Philippe Colletier, Diana Kirilovsky,\* Gotard Burdzinski,\* and Michel Sliwa\*



Cite This: *JACS Au* 2022, 2, 1084–1095



Read Online

ACCESS |



Metrics & More



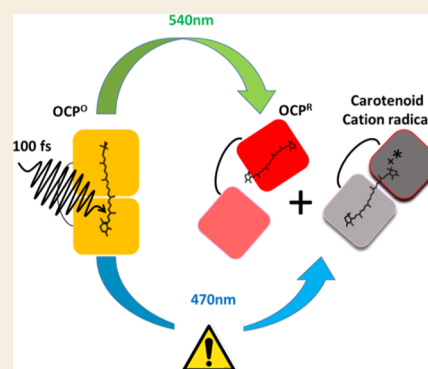
Article Recommendations



Supporting Information

**ABSTRACT:** A substantial number of Orange Carotenoid Protein (OCP) studies have aimed to describe the evolution of singlet excited states leading to the formation of a photoactivated form,  $OCP^R$ . The most recent one suggests that 3 ps-lived excited states are formed after the sub-100 fs decay of the initial  $S_2$  state. The  $S^*$  state, which has the longest reported lifetime of a few to tens of picoseconds, is considered to be the precursor of the first red photoproduct  $P_1$ . Here, we report the ultrafast photodynamics of the OCP from *Synechocystis* PCC 6803 carried out using visible–near infrared femtosecond time-resolved absorption spectroscopy as a function of the excitation pulse power and wavelength. We found that a carotenoid radical cation can form even at relatively low excitation power, obscuring the determination of photoactivation yields for  $P_1$ . Moreover, the comparison of green (540 nm) and blue (470 nm) excitations revealed the existence of an hitherto uncharacterized excited state, denoted as  $S^{\sim}$ , living a few tens of picoseconds and formed only upon 470 nm excitation. Because neither the  $P_1$  quantum yield nor the photoactivation speed over hundreds of seconds vary under green and blue continuous irradiation, this  $S^{\sim}$  species is unlikely to be involved in the photoactivation mechanism leading to  $OCP^R$ . We also addressed the effect of His-tagging at the N- or C-termini on the excited-state photophysical properties. Differences in spectral signatures and lifetimes of the different excited states were observed at a variance with the usual assumption that His-tagging hardly influences protein dynamics and function. Altogether our results advocate for the careful consideration of the excitation power and His-tag position when comparing the photoactivation of different OCP variants and beg to revisit the notion that  $S^*$  is the precursor of photoactivated  $OCP^R$ .

**KEYWORDS:** orange carotenoid protein, photodynamics, ultrafast spectroscopy, multiphoton absorption, cation radical, echinenone, quantum yield, His-tag



## INTRODUCTION

The Orange Carotenoid Protein (OCP) is a 35 kDa water-soluble photoactive protein capable of quenching the excess light energy harvested by cyanobacteria.<sup>1–4</sup> In order to perform its energy-quenching function, dark-adapted OCP (abbreviated as  $OCP^O$  due to its orange color) must be photoactivated by strong blue-green light illumination, yielding the  $OCP^R$  species capable of quenching excited phycobilisomes.<sup>5</sup> The protein is structured as a two-domain protein, where the N-terminal (NTD) domain is the effector, and the C-terminal (CTD) domain is the regulator.<sup>6,7</sup> The functionalizing ketocarotenoid chromophore is embedded at the interface between the NTD and CTD.<sup>8</sup> The main function of OCP is to quench the fluorescence of the cyanobacterial light-harvesting antennas, a.k.a., phycobilisomes. Only the  $OCP^R$  state can interact with the latter and perform the quenching function.

The photoactivation of  $OCP^O$  starts with the evolution of the chromophore excited-state levels resulting in the formation of  $P_1$ . This state is the first red photoproduct with broken H bonds between the carotenoid and the protein.<sup>9</sup> The 12 Å migration of the ketocarotenoid in the NTD<sup>10</sup> and structural changes in the protein, respectively, occurring in the microsecond and millisecond time scales, ultimately<sup>9,11,12</sup> lead to the separation of the two domains (Scheme 1a), yielding  $OCP^R$ . The photoconversion quantum yield of  $OCP^R$  is very low (0.2% or less),<sup>5,9,11,12</sup> reflecting the functional requirement that OCP remains inactive in low irradiance

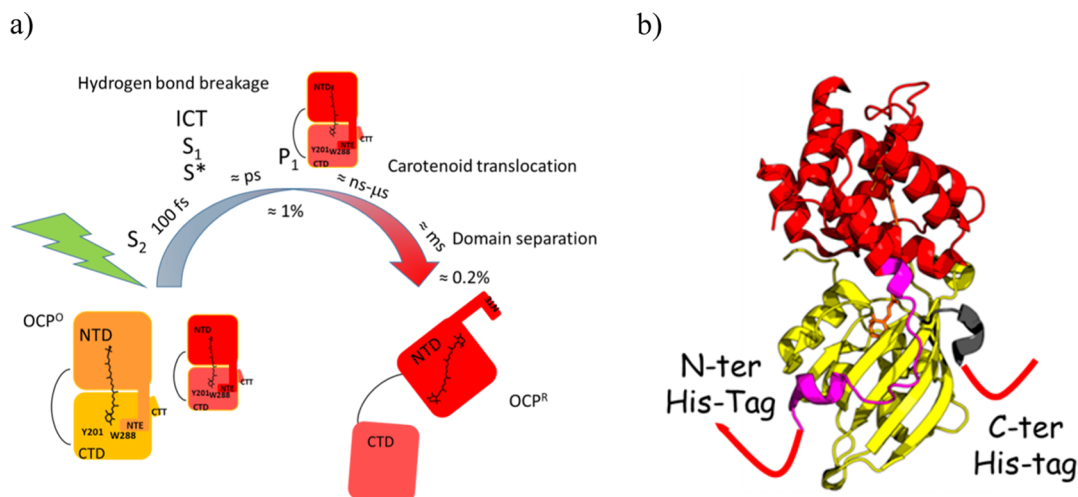
**Received:** October 22, 2021

**Revised:** February 2, 2022

**Accepted:** February 3, 2022

**Published:** April 25, 2022



Scheme 1. (a) General Photodynamical Scheme of OCP Photoactivation Mechanism<sup>a</sup>

<sup>a</sup>In the dark, two sub-populations of the closed OCP<sup>O</sup> are present, a “normal” one and a red-shifted one (the size represents their contribution, Figure S2 in Supporting Information). (b) OCP structure (reproduced from PDB ID 3MG1) comprises a fully  $\alpha$ -helical NTD, featuring a fold that is unique to cyanobacteria, whereas the CTD has a mixed  $\alpha/\beta$  architecture and belongs to the NTF-2 family.<sup>8</sup> His-tags can be attached to the N-terminal extension or to the C-terminal tail

conditions, that is, when maximum energy transfer to photochemical centers is needed. The low OCP photoconversion quantum yield is determined during excited-state deactivation, with about 99% of the ketocarotenoid relaxing back to the initial  $S_0$  state within tens of picoseconds.<sup>5,9,12,13</sup> The ultrafast photodynamics of different OCPs and carotenoids [hydroxyechinenone, echinenone (ECN), canthaxanthin, and zeaxanthin] have been studied by femtosecond transient absorption spectroscopy using various excitation wavelengths in the visible range.<sup>5,9,14–18</sup> The most recent studies consider that upon the relaxation of the initial  $S_2$  state, 3 ps-lived excited states are formed: a sub-picosecond-lived intramolecular charge-transfer (ICT) state, a picosecond-lived mixed  $S_1$ /ICT state called usually  $S_1$ , and an excited state  $S^*$  characterized by a lifetime in the range of few picoseconds<sup>13</sup> to few tens of picoseconds,<sup>9</sup> depending on the source. There is a longstanding debate regarding the ground *versus* excited-state nature of the carotenoid  $S^*$  state but no agreement has been reached thus far.<sup>19–22</sup> Carotenoid  $S^*$  was first postulated to be a hot ground state,<sup>19</sup> then redefined as an electronically excited state,<sup>20</sup> but some publications questioned this hypothesis and pointed out different properties, featuring a vibrationally hot electronic ground state.<sup>21–24</sup> Regardless, the ICT,  $S_1$ , and  $S^*$  populations are all known to decay within few tens of picoseconds, while the first red photoproduct  $P_1$  appears with a yield of about 1.5%.<sup>9</sup> Despite this already vast knowledge, the low magnitude of the  $P_1$  signal implies that a high error intrinsically exists on the determined quantum yield. Furthermore, it remains unclear, which of the excited states, are the precursor of  $P_1$ . Recent studies have considered  $S^*$ , on the basis that  $S^*$  would have a distorted geometry, which favors the breaking of the hydrogen bond and formation of  $P_1$ .<sup>9</sup> However, the issues concerning the genuine nature of  $S^*$  render any firm conclusion difficult.

Kennis and co-workers were the first to report that the formation yield and lifetime of the  $S^*$  state depend on the excitation peak power.<sup>9</sup> Such results could be explained by the existence of additional pathways and extra species, possessing similar spectra but different lifetimes and generated by

multiphotonic processes caused by femtosecond pulse excitation—as reported for other photoactive proteins.<sup>25,26</sup> Multiphotonic processes are usually accompanied by off-pathway species, such as radical cations and solvated electrons, which are avoided when the excitation pulse is stretched or the excitation energy reduced.<sup>25,26</sup> The Polivka group showed an increase of the  $S^*$  population and the existence of a long-lived radical signal peaking at 900 nm, when probing the effect of UV excitation on canthaxanthin-functionalized OCP.<sup>27</sup> A functional role of an oxocarbenium cation was even suggested in the photoactivation of OCP<sup>O</sup>.<sup>13</sup> Surprisingly, despite the fact that the low energy keto-carotenoid absorption band is associated with the  $S_0 \rightarrow S_2$  transition, no studies have investigated the power dependence of excitation using femtosecond pulses thus far. Clearly, knowledge of the photoexcitation power dependence and characterization of radical cations is crucial for the interpretation of OCP ultrafast dynamics. Also, two excitation wavelengths have been used depending on studies, *viz.*, 470 and 540 nm,<sup>14,16,28</sup> due to the existence of at least two ground-state populations in the dark form (referred to as “normal” and “red-shifted”<sup>14,29</sup>). The 540 nm excitation presumably selects only the red-shifted sub-population, while 470 nm excites both of them. Last, studies have been performed on the C-tagged or N-tagged OCPs,<sup>5,9,14–18</sup> yet the (admittedly unlikely) hypothesis that tagging could influence ultrafast photodynamics was never investigated, despite both tags being located on helices attached to the sensory domain, that is, the CTD (Scheme 1). It could thus be that tagging affects the equilibrium between the normal and red-shifted dark-adapted OCP<sup>O</sup> (Scheme 1) and/or their excited-state dynamics, which could in turn influence the photoconversion yield.

Here, we report a detailed photophysical study on OCP from *Synechocystis* PCC 6803 complexed with the ketocarotenoid ECN. The use of visible–near infrared (NIR) femtosecond transient absorption spectroscopy allowed to identify all species involved in the OCP excited-state deactivation. With an aim to afford a comparison with all previously published transient spectroscopy studies,<sup>5,9,14–18</sup> we

investigated light-induced excited-state dynamics upon excitation by either 470 or 540 nm light. Stationary irradiation experiments were also performed at the two excitation wavelengths. Both on the C-tagged or N-tagged variants of OCP were studied, to test the effect of the tag and its position on ultrafast photodynamics. On each construct and at the two wavelengths, we furthermore probed the effect of the excitation power on excited-state dynamics. We show how the picosecond dynamics that determines the formation of  $P_1$ , the first crucial intermediate controlling the formation quantum yield of  $OCP^R$ , are influenced by the excitation energy and wavelength. The combination of transient absorption and stationary irradiation experiments upon 470 and 540 nm excitation allows us to identify which of the picosecond-lived states correlates with the final photoactivation quantum yield and is thus the most likely candidate to be the precursor of  $P_1$ . We show that the use of high excitation power leads to the formation of a carotenoid radical cation, whose presence may result in an erroneous extraction of  $P_1$  yield from OCP bleach kinetics. Finally, we demonstrate that upon 470 nm excitation the photodynamics of OCP feature a yet unidentified  $S^*$  state whose existence may compromise the estimation of the  $S^*$  lifetime and  $P_1$  yield. Taking into account all the above-mentioned aspects of OCP photoexcitation will prove crucial, not only to understand the basis for the biological function of OCP but also to design OCPs with a higher photoactivation quantum yield.

## MATERIALS AND METHODS

### Protein Expression and Purification

The plasmid pCDF-NtagOCPsyn used for the expression of OCP from *Synechocystis* PCC 6803 carries a sequence coding for a His-tag in the N terminus and was characterized in de Carbon *et al.*<sup>30</sup> The expression of the OCP genes in *Escherichia coli* cells containing the genes for the synthesis of ECN and the isolation of ECN-OCP was also described.<sup>30</sup> The expression of the OCP genes in *Synechocystis* was reported by Gwizdala *et al.*<sup>31</sup> N-tagged OCP was expressed in *E. coli*, while C-tagged OCP was expressed in the  $\Delta$ crtR *Synechocystis* mutant lacking zeaxanthin and hydroxyechinenone. Exactly the same N-tagged OCP was used in Konold *et al.* (same protein expression and purification procedure).<sup>9</sup> The protein concentration used in the experiments described in this work was close to 1 mg/mL (calculated using absorbance at 496 nm) and 40 mM Tris–HCl 25 mM NaCl pH 8.0 buffer was used.

### Steady-State UV–Vis Absorption Spectra and Photoconversion under Steady-State Irradiation

Steady-state UV–vis absorption spectra were recorded with a Jasco V-550 spectrophotometer, using 2 nm spectral bandwidth. The cuvette optical path was 10 mm for stationary LED irradiation spectroscopy experiments. The photoconversion kinetics set up is described elsewhere.<sup>32</sup> Here, the photoactivation was induced by green LED irradiation [ $\lambda_{\max} = 528$  nm, full width at half maximum (FWHM) = 28 nm, standard 3 W emitter], and blue LED irradiation ( $\lambda_{\max} = 470$  nm, FWHM = 18 nm, standard 3 W emitter). The probing and irradiation beams were at 90°. The optical irradiation path of the solution was 4 mm and the probing path was 10 mm. The absorbances at 470 and 528 nm were the same for C-tagged and N-tagged OCP (0.53 and 0.28 for 470 and 528 nm, respectively). The irradiation power was 3.4 mW/cm<sup>2</sup> for the blue LED and 3.0 mW/cm<sup>2</sup> for the green LED, therefore the photon flux is the same in both cases.

### Femtosecond Vis–NIR Transient Absorption

Femtosecond vis–NIR transient absorption spectra were collected using a commercially available system (Ultrafast Systems, Helios) described previously<sup>33</sup> that consists of a short-pulse titanium-sapphire

oscillator (Mai-Tai, Spectra Physics, 70 fs) followed by a high-energy titanium-sapphire regenerative amplifier (Spitfire Ace, Spectra Physics, 100 fs, 1 kHz). The 800 nm beam was split into two beams to generate as follows: (1) the pump ( $\lambda_{\text{exc}} = 540$  or 470 nm) in the optical parametric amplifier (Topas Prime with a NirUVVis frequency mixer) and (2) probe pulses—white light continuum in the vis–NIR range generated by focusing the fundamental beam into a sapphire (430–780 nm) or YAG (820–1390 nm) crystal. The remaining 800 nm probe pulse photons were filtered. The instrument response function (IRF) was determined by fitting the kinetics of the coherent artefact signal from the solvent and was estimated to be  $\approx 110$  fs (FWHM). The experiments were performed with different pulse energies ranging from 0.2  $\mu$ J ( $3.3 \times 10^{14}$  photons per cm<sup>2</sup> at FWHM) up to 1.6  $\mu$ J upon 470 nm excitation and from 0.4  $\mu$ J ( $6.6 \times 10^{14}$  photons per cm<sup>2</sup> at FWHM) up to 3.2  $\mu$ J upon 540 nm excitation using variable neutral density filters. The pump diameter (FWHM) at the sample was  $\approx 250$   $\mu$ m. Numbers of photons and fluence per pulse are given in the Supporting Information (Figures S5 and S6). In all transient absorption experiments, the absorbance was close to 0.7 at the excitation wavelength in a 2 mm optical path. The sample solution was stirred to keep fresh OCP solution in the probed volume. The transient spectra were registered with 1 nm per pixel and by averaging 500 supercontinuum spectra with and without excitation, respectively. The entire set of the pump–probe time delay points was repeated four times to ensure data reproducibility, then the data were inspected and averaged. Moreover, to ensure that all data sets are comparable to each other, they were measured in one experimental session, in identical conditions except for varied parameters (like pump energy, explicitly given). The pump beam was depolarized to avoid anisotropy effects. The sample temperature was set to 22 °C. The stability of the sample was checked by comparing the stationary UV–vis absorption spectra measured before and after the experiments.

### Data Analysis

The transient absorption data were corrected for the chirp of white light continuum based on the given amount of sapphire, water, and BK7 glass, which the probe pulse had to pass through. Afterward, visible and NIR data were merged using a custom procedure.<sup>33</sup> Low intensity of the probing pulse and presence of a relatively strong residual 800 nm beam (even after filtering) resulted in minor artefacts visible in recorded data around 800 nm. For all data sets, the difference absorbance value obtained at the bleaching extremum (in both spectral and temporal dimension) was normalized to  $-1$ . Transient spectra were projected onto a 5 nm-spaced grid to get kinetic traces. The comparison of pre-exponential factors at 490 nm (bleaching band) allowed us to estimate the formation quantum yield of the various intermediates. Data processing to determine time constants and decay-associated difference spectra (DADS or DAS) was based on our custom fitting procedure.<sup>34</sup> It consists of two steps. (i) First, it fits globally (time constants are shared) kinetics at representative wavelengths (480, 490, 500, 570, 590, 610, 655, 740, 960, and 1100 nm) with convolution (IRF 110 fs FWHM) and weights (to increase the contribution of the long delays, which are our main interest, to the  $\chi^2$  error term). The following weights were used: 1.0 under 0.25 ps, 2.5 between 0.25 and 8 ps, 7.5 between 8 and 12 ps, and 12.5 after 12 ps. (ii) In the second step, time constants extracted from the first step are fixed and used to fit all kinetics separately (again with the same weights and convoluted with IRF), and finally DAS are built from obtained pre-exponential factors. The spectral and temporal ranges of the fit (the same for both steps) are 430 to 1380 nm and  $-1$  ps to 1 ns, respectively. Bootstrapping analysis was also performed to estimate errors (see the Supporting Information for more details). We also tested our results against other procedures, like the one implemented in the Glotaran package.<sup>35</sup> To fit data sets with 540 nm excitation, we used a sum of four exponential terms plus an offset (representing long-lived photoproducts,  $> 10$  ns, namely,  $P_1$  and carotenoid radical). For data sets excited with a 470 nm pulse, it was required to apply an additional component, so in this case there were five exponential terms plus the offset.



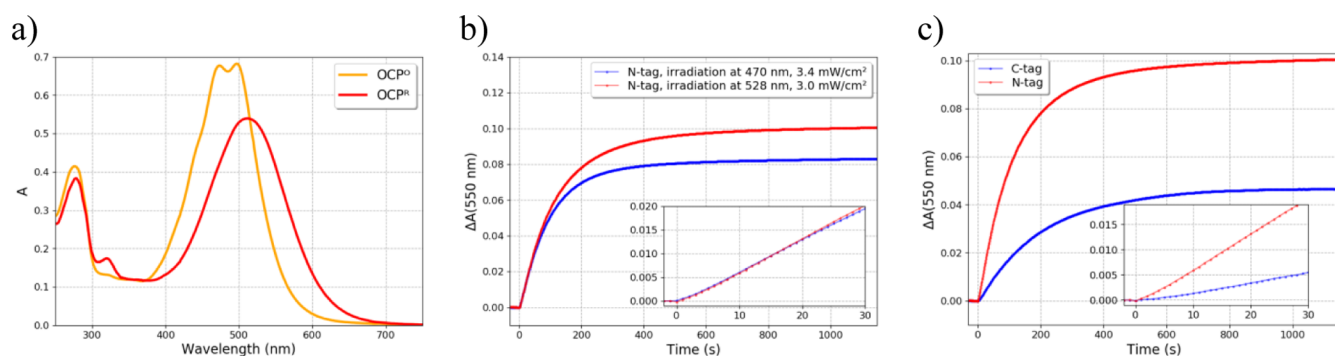


**Figure 1.** (a) UV–vis stationary spectra of  $\text{OCP}^{\text{O}}$  (recorded in the dark) and  $\text{OCP}^{\text{R}}$  (under 452 nm irradiation, 3.2  $\text{mW}/\text{cm}^2$ ), 1 cm path length, 11 °C. (b) Evolution of  $\Delta A$  at 550 nm (22 °C) for N-tagged OCP (N-tag) upon 528 nm (FWHM = 28 nm, 3.0  $\text{mW}/\text{cm}^2$ ) and 470 nm (FWHM = 18 nm, 3.4  $\text{mW}/\text{cm}^2$ ) LED irradiation and (c) comparison of C-tagged (C-tag) and N-tagged (N-tag) OCP upon 528 nm LED irradiation. Initial slopes are shown in the insets.

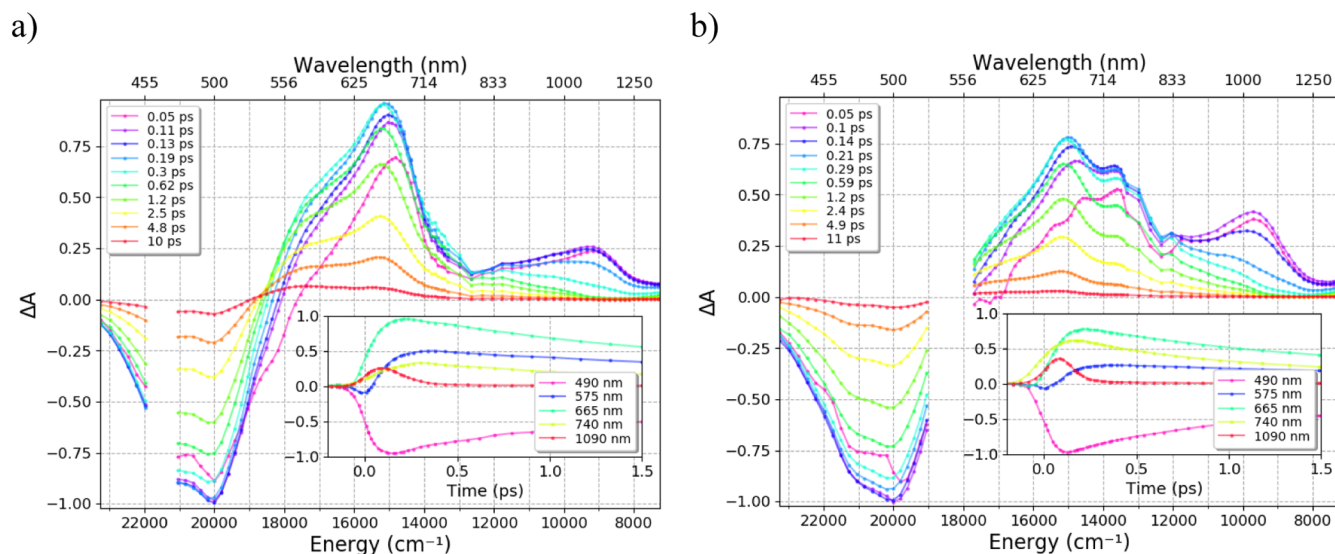


**Figure 2.** Transient absorption spectra between 0.05 and 10 ps of N-tagged OCP excited at (a) 470 nm (0.4  $\mu\text{J}$ ) and (b) 540 nm (0.8  $\mu\text{J}$ ). All data sets were normalized to  $-1$  at the bleaching extremum (in both spectral and temporal dimensions). To obtain the original signal, multiply plotted values by (a) 0.077 and (b) 0.088. Insets show evolution of the signal in the 1.5 ps time window.

## RESULTS

### Steady-State Properties

In the  $\text{OCP}^{\text{O}}$  (dark-adapted) state, UV–visible absorption spectra of N-tagged and C-tagged OCP show almost no difference, both display a broad absorption band, characteristic of the  $S_0$ – $S_2$  transition, with two maxima at 472 and 496 nm and a tail until 650 nm (Figures 1a, S1 in Supporting Information).<sup>29,36</sup> The “red-shifted” population was estimated by Gaussian decomposition to be around 20% for both N-tagged and C-tagged OCPs (Figure S2), in line with previous reports.<sup>14</sup> To determine if a difference in the ability to photoactivate exists between the two dark-adapted sub-populations, N-tagged and C-tagged OCP solutions (same absorbance) were irradiated with blue (470 nm LED) and green (528 nm LED) light, thereby selecting either the “normal” or the “red-shifted” sub-populations of  $\text{OCP}^{\text{O}}$ . The initial slope of the evolution of the absorbance at 550 nm (Figure 1b), which probes the formation of  $\text{OCP}^{\text{R}}$ , shows that both sub-populations of N-tagged OCPs photoactivate with the same efficiency when using different irradiation wavelengths. There is a slight difference in the photostationary state (achieved approximately after 600 s of LED irradiation),

suggesting that 528 nm irradiation ultimately generates quantitatively more  $\text{OCP}^{\text{R}}$ . This result can be explained by a deviation from dark-adapted equilibrium between sub-populations in the  $\text{OCP}^{\text{O}}$  state, caused by an extended period of irradiation (e.g., 528 nm selects one sub-population, but photoactivated OCPs may repopulate both sub-populations after back-conversion). Unexpectedly, the comparison of the evolution of the absorbance traces at 550 nm for the different tags (Figure 1c) reveals a much faster photoactivation of N-tagged OCP than C-tagged OCP (the initial slope is 3.5 times larger for the N-tagged OCP). This difference in  $\text{OCP}^{\text{R}}$  yield could stem either from different excited-state dynamics, leading to different  $P_1$  formation quantum yield, or from changes in the yield of subsequent ground-state species forming in the ns–ms time scale (Scheme 1, carotenoid translocation and domain separation dynamics).<sup>9,11,12</sup> To split a difference between the two hypotheses, a more detailed analysis of the early stages of the photoinduced processes is needed.

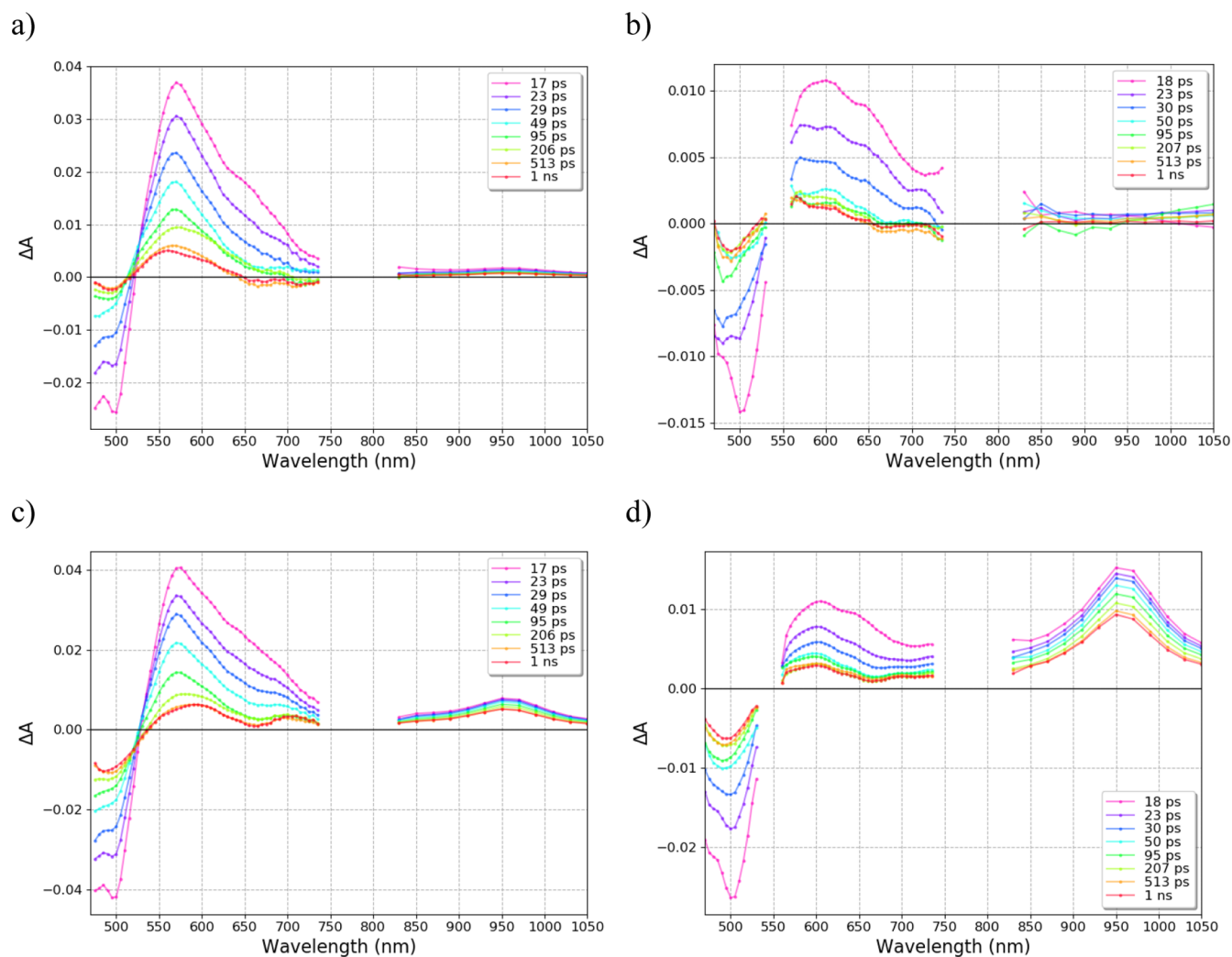


**Figure 3.** Transient absorption spectra between 17 ps and 1 ns for N-tagged OCP excited at (a) 470 nm ( $0.4 \mu\text{J}$ ), (b) 540 nm ( $0.8 \mu\text{J}$ ), (c) 470 nm ( $1.6 \mu\text{J}$ ), and (d) 540 nm ( $3.2 \mu\text{J}$ ). All data sets were normalized to  $-1$  at the bleaching extremum [in both spectral and temporal dimensions, multiply by (a) 0.077, (b) 0.088, (c) 0.163, and (d) 0.234 to get original signal].

### Femtosecond Transient Absorption Spectroscopy of N-Tagged OCP

The ultrafast photodynamics of N-tagged OCP was studied upon 470 and 540 nm excitation wavelengths. The excitation pulse energy was initially set to  $0.4 \mu\text{J}$  at 470 nm and to  $0.8 \mu\text{J}$  at 540 nm, which ensures being in the linear photoexcitation range (Figure 4), while getting enough S/N to characterize  $P_1$  and keeping the data free of additional signals arising when higher energy is used (detailed discussion in the next section). Figure 2 shows femtosecond transient absorption data recorded with 470 and 540 nm excitation, respectively. Just after 540 nm excitation, at 0.05 ps, a primary positive absorption band peaking at 1050 nm is observed. This band is assigned to the  $S_2$  excited-state population ( $S_2 \rightarrow S_n$  transition).<sup>17</sup> The band is broader upon 470 nm excitation and its maximum is shifted to 1100 nm, indicating the presence of an excess of vibrational energy and pointing to the excitation of a larger range of OCP<sup>0</sup> sub-populations. Concomitant with the formation of the  $S_2$  state within 50 fs, a ground-state bleaching (GSB; indicative of OCP<sup>0</sup> depopulation) signal is observed in the visible region (see Figure S3, which is zooming into the visible region), with a maximum at about 500 nm, as well as the appearance of two main excited-state absorption

(ESA) bands, at about 663 and 740 nm (Figures 2, S3). These two ESA can be assigned to the  $S_1$  and ICT states.<sup>14,15</sup> In addition to the ICT and  $S_1$  states, the shoulder around 570 nm can be assigned to the  $S^*$  state in agreement with the recent literature.<sup>9,13</sup> After 50 femtoseconds, the first signal evolution is the decay of the  $S_2$  state within a few hundreds of femtoseconds. During this time, the ESA bands attributed to  $S_1$  and  $S^*$  states continue to grow slightly until 0.2 ps. The amplitudes of the bands around 570–585 nm ( $S^*$  contribution) and 663 nm ( $S_1$  contribution) are higher for the 470 nm excitation. Conversely, and in agreement with previous results,<sup>14,15,28</sup> the ICT character is more pronounced when 540 nm excitation is used, resulting in higher amplitude signals around 740 nm and a long tail up to 1100 nm. This increase in the amplitude of the ICT character is at the expense of the amplitudes of the bands at 663 and 570 nm. After 10 picoseconds, the  $S_1$  and ICT states decay concomitant to recovery of 97% of the GSB band (Figure 2). At 23 ps time delay, the remaining signal is characterized by the broad positive absorption band usually assigned to the  $S^*$  state, with a maximum at 570 nm and a shoulder around 655 nm (Figure 3).<sup>9</sup> The comparison of the transient spectra at 23 ps recorded after 470 and 540 nm excitations, respectively (Figure 3a,b,

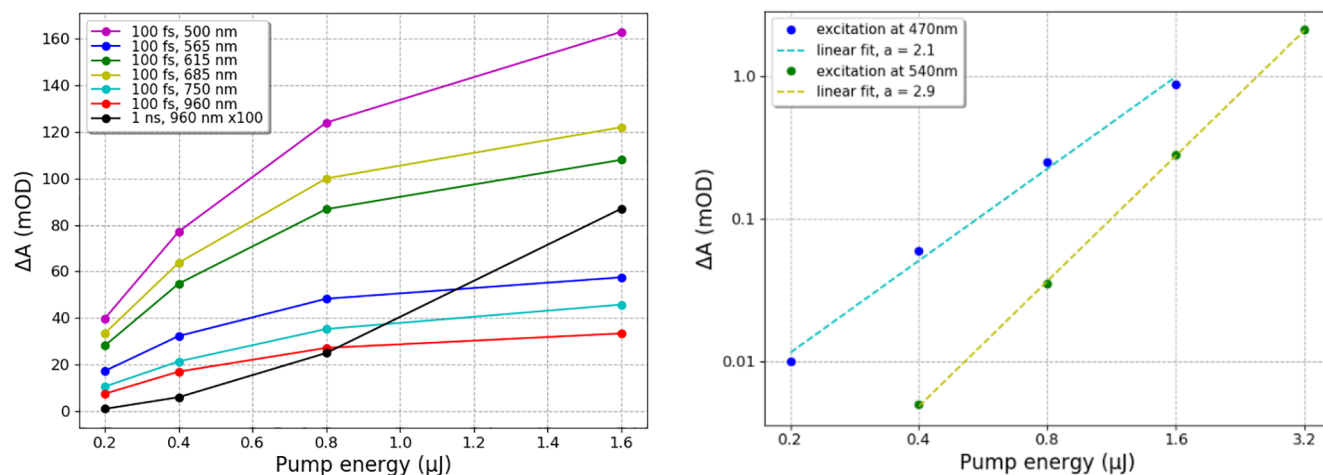


**Figure 4.** (a) Difference absorbance value at different wavelengths *versus* pump energy for 470 nm excitation (the value at 500 nm was multiplied by  $-1$ ) and (b) log–log plots of cation radical absorbance (960 nm) at 1 ns time delay *versus* excitation energy upon 470 and 540 nm excitation.

purple spectrum), reveals major differences, the most notable one being that the GSB band is two times smaller for 540 nm excitation (about 0.008 *vs* 0.016 for 540 and 470 nm excitations; values estimated from the GSB signal at 490 nm). Moreover, while the transient absorption band observed upon 470 nm excitation peaks at 570 nm, that observed upon 540 nm excitation has a much broader shape, with the maximum shifted to  $\approx 585$  nm and a much higher amplitude of the shoulder around 655 nm. Thus, both excitations lead to different  $S^*$ -type species. The  $S^*$  state decays within 50 ps; however, upon 470 nm excitation there is an extra time evolution of the 570 nm band within 500 ps (Figure 3a). This is assigned to the existence of an additional species  $S^{\sim}$ , forming only upon 470 nm excitation and characterized by a positive absorption band with a maximum located at 570 nm and a lifetime of *ca.* 80 ps. Finally, irrespective of the excitation wavelength, the transient absorption spectrum at 1 ns is characterized by a GSB of  $OCP^O$  of similar intensity yet a broad positive band also remains, with a maximum at  $\approx 565$  nm, which is broader and two times higher in amplitude when a 470 nm pump is used. This band is assigned to  $P_1$ ; however, only the GSB band, corresponding to  $OCP$  molecules that have not relaxed to the initial  $OCP^O$  state, can afford the estimation of the  $P_1$  yield. Thus, using the GSB band of  $OCP^O$  at 490 nm and taking into account the positive absorbance contribution from  $P_1$  at 490 nm (see Supporting Information, Figure S4),  $P_1$  formation quantum yields are estimated to be  $\approx 0.5\%$  for both excitations. These results are also in accordance with the photoactivation efficiency being independent of the irradiation wavelength (470 or 528 nm, Figure 1a).

#### Effect of High Energy Pump Pulse Excitation

Power dependence measurements were done in the energy range of 0.2–1.6  $\mu J$  for 470 nm and 0.4–3.2  $\mu J$  for 540 nm excitation. Transient absorption spectra for 1.6  $\mu J$  (470 nm) and 3.2  $\mu J$  (540 nm) are shown for short time delays in the Supporting Information (Figure S7) and presented in Figure 3c,d for time delays between 17 ps and 1 ns. It should be noted that higher energies were also explored; however, fast sample degradation was observed as well as an increase in the scattering of the excitation beam. For the highest pulse energy, the number of photons absorbed per chromophore in the

center of the beam was close to 0.8 (Figures S5 and S6). Figure 3 shows that at 1 ns time delay (Figure 3a,b) only  $P_1$  is present for low excitation energies (positive band with a maximum at 565 nm), while additional positive absorption bands at 700 and 960 nm (Figure 3c,d), characteristic of the radical cation species of the carotenoid,<sup>37,38</sup> are observed for high excitation energies. A minor contribution is also present at 600 nm, overlapping with the  $P_1$  absorption band (compare Figure 3a,c at 1 ns time delay). The presence of a radical cation is characterized by an increase in the depopulation (GSB) band extremum value *versus* pulse excitation energy (band at 500 nm), while the maximum value of absorbance for  $S^*$ ,  $S_1$ , and ICT states (565/685/750 nm) reaches a plateau for excitation energies exceeding 0.8  $\mu J$  for 470 nm and 1.6  $\mu J$  for 540 nm (Figure 4a). The radical cation signal also affects the  $P_1$  positive absorption band, although to a lesser extent than the GSB band, which peaks to 1% depopulation of  $OCP^O$  when excitation energy reaches 1.6  $\mu J$  upon 470 nm excitation (Figure 3c). The thresholds for the observation of the radical cation are 0.4 and 0.8  $\mu J$  at 470 and 540 nm, respectively, with the signal at 960 nm being negligible at these excitation energies (Figure 4). These were therefore selected to characterize the photodynamics of  $OCP$  with the best possible S/N ratio, while avoiding contribution of biologically irrelevant species. Figure 4b shows a log–log plot of absorbance at 960 nm and 1 ns time delay *versus* excitation energy, underlining the multiphotonic nature of the process leading to the formation of the radical cation. Indeed two photons are involved in the formation of the radical for 470 nm excitation (a slope of two points to a purely biphotonic character, doubling pump pulse power causes fourfold increase in a radical signal) and three photons for 540 nm excitation (Figure 4b). The detailed effects of multiphoton excitation on the different excited states (formation quantum yield and lifetime) can be assessed by multi-exponential analysis, discussed in the next section.

#### Global Analysis of Transient Absorption Data in the Linear and Nonlinear Excitation Regime

For the 540 nm data sets, four exponential components convoluted with a Gaussian-shaped pulse of 110 fs (FWHM) and an offset for long-lived photoproducts ( $>10$  ns) are required to obtain a quality fit of all kinetic traces. These



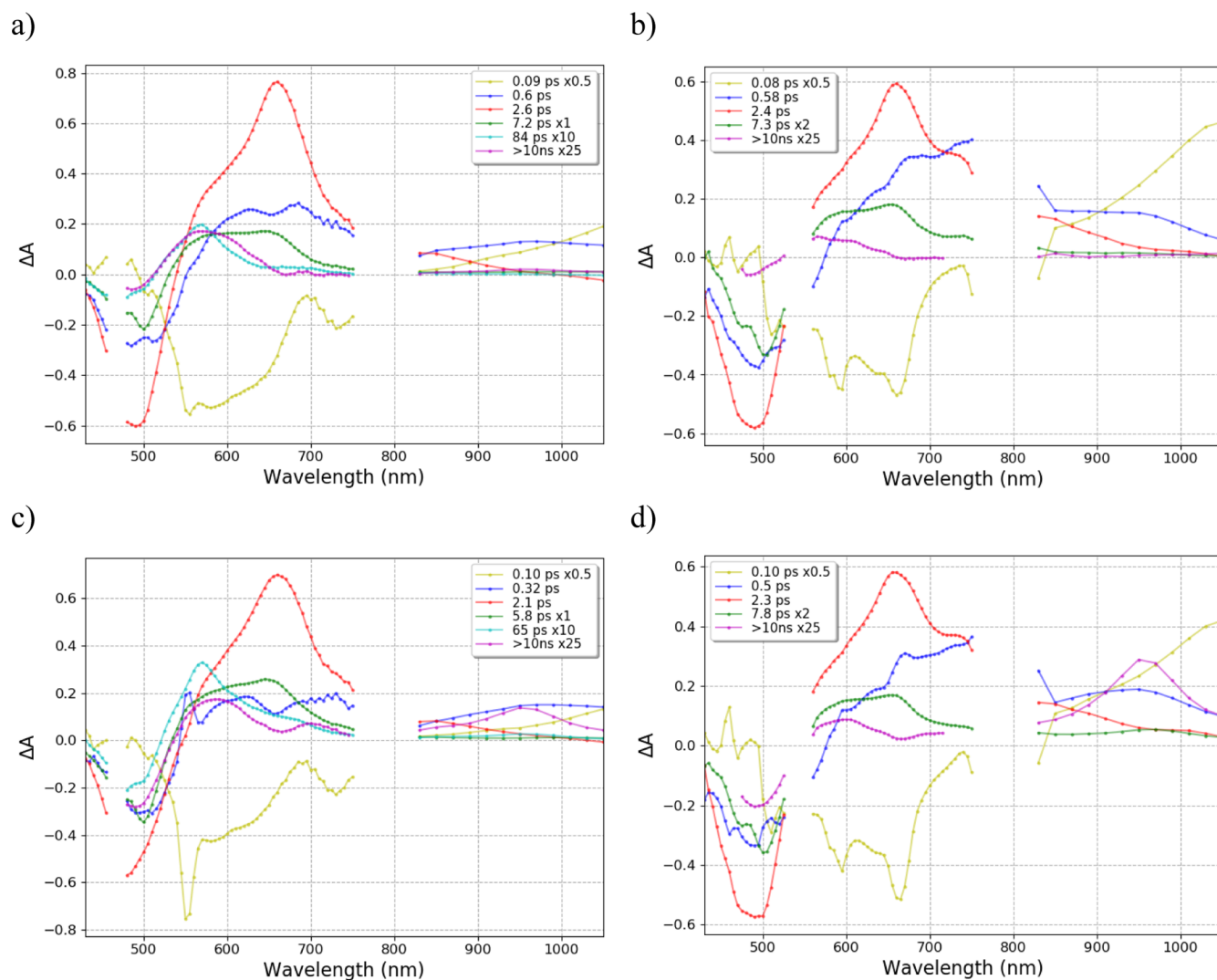


**Figure 5.** DAS obtained from the global fit of transient absorption data recorded for N-tagged OCP with excitation at (a) 470 nm, 0.4  $\mu$ J, (b) 540 nm, 0.8  $\mu$ J, (c) 470 nm, 1.6  $\mu$ J, and (d) 540 nm, 3.2  $\mu$ J. DAS shown in green are multiplied by 2 for 540 nm excitation and DAS shown in yellow and in magenta are multiplied by 0.5 and 25 for both excitations.

components provide four characteristic time constants that can be used to describe the behavior of the different excited states ( $S_2$ , ICT,  $S_1$ , and  $S^*$ ) and the long-lived photoproduct  $P_1$ , populated in the end of our time window (1 ns). As already mentioned, for 470 nm excitation, one additional component is needed, which is denoted as  $S^{\sim}$  (see Figure S8). For all data sets, the first component around 100 fs is associated with the  $S_2$  state, and also includes the growth of  $S_1$ , ICT, and  $S^*$ , overlapped with artefacts such as stimulated Raman and eventually any ultrafast intramolecular vibrational relaxation.

The decay associated spectra (5 exponential components for 470 nm and 4 exponential components for 540 nm excitation) for low energy excitation, 0.4  $\mu$ J at 470 nm and 0.8  $\mu$ J at 540 nm, are shown in Figure 5a,b. Kinetic traces of the representative wavelengths with their fits and residuals are given in Figures S9 and S11 (Figure S16 zooms in on the  $-0.25$  to 1 ps time delay window). The decay associated spectra for both excitations represent  $S_2$  (yellow), ICT (blue),  $S_1$  (red),  $S^*$  (green),  $S^{\sim}$  (cyan, only for 470 nm excitation), and  $P_1$  (magenta) species (Figure 5) with associated time constants around  $0.6 \pm 0.08$ ,  $2.5 \pm 0.36$ ,  $7.0 \pm 2.3$ , and  $80 \pm 30$  ps (retrieved time constants are provided in Table 1,

standard errors calculated from bootstrapping distributions in Tables S2 and S3). For both excitations, the  $S^*$  state has a lifetime of about 7 ps with a spectrum characterized by a maximum at 655 nm and a shoulder at 585 nm. The  $S^{\sim}$  state, which has a longer lifetime of about 80 ps, has its absorption maximum at 570 nm and is similar in shape to the  $S^*$  state reported by Konold *et al.*<sup>9</sup> ( $\lambda_{\text{exc}} = 475$  nm). This component is not observed for 540 nm excitation. Global analysis with four exponential components (Figures S14 and S15) was also performed for the 470 nm excitation data sets (see the comparison of DAS for four and five exponential components in Figure S15); however, a structure in residuals appears between 10 and 100 ps (Figure S14), and the resulting DAS of the  $S^*$  state has significantly different properties compared to the ones obtained after 540 nm excitation. In other words, the addition of the  $S^{\sim}$  component for the 470 nm data set is indispensable to obtain a consistent description of the results recorded with both excitations. Note that time constants retrieved from four exponential fits of the 470 nm excited data set are in agreement with those reported earlier by Konold *et al.*,<sup>9</sup> suggesting that this component was already present, but

**Table 1. Lifetimes and Estimated Formation Quantum Yields from Pre-exponential Factors at 490 nm for ICT/S<sub>1</sub>/S\*<sup>•</sup>/S<sup>•</sup>/P<sub>1</sub> States (See Supporting Information for Details and Table S1)<sup>a</sup>**

	ICT	S <sub>1</sub>	S* <sup>•</sup>	S <sup>•</sup>	P <sub>1</sub> <sup>b</sup>
N-tag 470 nm/0.4 μJ	25.8%	57.1%	16.5%	0.7%	0.5%
	0.60 ps	2.6 ps	7 ps	80 ps	
N-tag 470 nm/1.6 μJ	26.5%	46.4%	25.5%	1.6%	2.4%
	0.32 ps	2.1 ps	6 ps	70 ps	
N-tag 540 nm/0.8 μJ	34.1%	53.7%	12.2%		0.5%
	0.58 ps	2.5 ps	7 ps		
N-tag 540 nm/3.2 μJ	31.6%	54.4%	14%		1.7%
	0.50 ps	2.4 ps	8 ps		
C-tag 540 nm/0.8 μJ	34.8%	53.9%	11.3%		0.6%
	0.44 ps	1.9 ps	6 ps		

<sup>a</sup>The following standard errors were estimated (see Supporting Information for details, Table S2 and S3):  $\tau_{\text{ICT}} \pm 80$  fs,  $\tau_{\text{S}_1} \pm 0.36$  ps,  $\tau_{\text{S}^*} \pm 2.3$  ps,  $\tau_{\text{S}^{\bullet}} \pm 30$  ps,  $A_{\text{ICT}} \pm 5\%$ ,  $A_{\text{S}_1} \pm 1.9\%$ ,  $A_{\text{S}^*} \pm 5\%$ ,  $A_{\text{S}^{\bullet}} \pm 1\%$ , and  $A_{\text{P}_1} \pm 0.1\%$ . <sup>b</sup>Note that for P<sub>1</sub> yield is corrected for its positive absorbance contribution at 490 nm (Figure S4) but not for interfering radical species at high power. <sup>c</sup>This P<sub>1</sub> yield represents a fraction of initially populated excited states, which reach P<sub>1</sub> state at 1 ns. The sum of ICT, S<sub>1</sub>, S\*<sup>•</sup>, and S<sup>•</sup> formation yields without P<sub>1</sub> equals 100% (because they represent branching from the S<sub>2</sub> precursor). More details can be found in the Supporting Information.

not identified, in their experiments carried out on the N-tagged protein using 475 nm excitation at 0.4 μJ excitation energy.

The detailed analysis of the DAS extracted from data collected at low excitation energies (0.4 μJ at 470 nm and 0.8 μJ at 540 nm) reflects the differences in amplitude and shape that were already observed in the raw data. (i) For ICT and S<sub>1</sub> states, the value of absorbance above 700 nm is higher for 540 nm excitation. These results were already reported in the literature<sup>14,15,28</sup> and can be explained by a more pronounced charge-transfer character of the S<sub>1</sub> and ICT states formed after 540 nm excitation (which is clearly visible in Figure 2). (ii) The absorbance of the S\*<sup>•</sup> state at 655 nm is about two times higher for  $\lambda_{\text{exc}} = 470$  nm. (iii) The absorbance at 663 nm for

the S<sub>1</sub> state is substantially higher for  $\lambda_{\text{exc}} = 470$  nm, while for the bleaching extremum (490 nm) it is almost the same for both excitations. (iv) A similar remark can be made for the maximum absorbance of P<sub>1</sub> (>10 ns DAS) at 565 nm, higher for 470 nm excitation, while at 490 nm the amplitude is similar for both excitations, pointing to a similar depletion of the OCP<sup>0</sup> state. However, it needs to be noted that the comparison of the magnitude of the P<sub>1</sub> positive absorption bands is difficult due to the scattered laser contribution in the 540 nm excitation data set.

As pointed above, P<sub>1</sub> formation quantum yields can be determined by using the GSB of OCP<sup>0</sup> depopulation band at 490 nm. A similar method can be used to determine yields of the excited states, which can be estimated from pre-exponential factors at 490 nm (associated with OCP<sup>0</sup> recovery, Table S1), divided by the sum of these excluding P<sub>1</sub> and S<sub>2</sub> (see Supporting Information for details and Table S1), with results shown in Table 1. It should be underlined here that such approximation assumes that (i) S<sub>1</sub>, ICT, and S\*<sup>•</sup> (and S<sup>•</sup> in case of 470 nm excitation) are formed from S<sub>2</sub> in parallel paths ((see discussion section)), (ii) these states decay mainly to S<sub>0</sub> without any interconversion, and (iii) their ESA is small at 490 nm. A comparison of 470 nm excitation (0.4 μJ) and 540 nm excitation (0.8 μJ) indicates a higher and lower contribution of the ICT (34% vs 26%) and S\*<sup>•</sup> state (12% vs 17%), upon excitation at 540 nm excitation. Meanwhile, the S<sub>1</sub> and P<sub>1</sub> formation quantum yields are independent of the excitation wavelength.

For the high excitation energy data sets, DAS for 1.6 μJ at 470 nm and 3.2 μJ at 540 nm are shown in Figure S5c,d, respectively (kinetic traces for representative wavelengths with their fit and residues are given in the Supporting Information, Figures S10 and S12). While the time constants for the S<sub>1</sub>/S\*<sup>•</sup>/S<sup>•</sup> states do not change with increasing excitation energy, the lifetime of the ICT state slightly decreases with a more pronounced effect observed for 470 nm excitation. The absorbance of positive contribution for excited states does not evolve significantly with an increase of the excitation energy. The most relevant feature is that the use of high energy

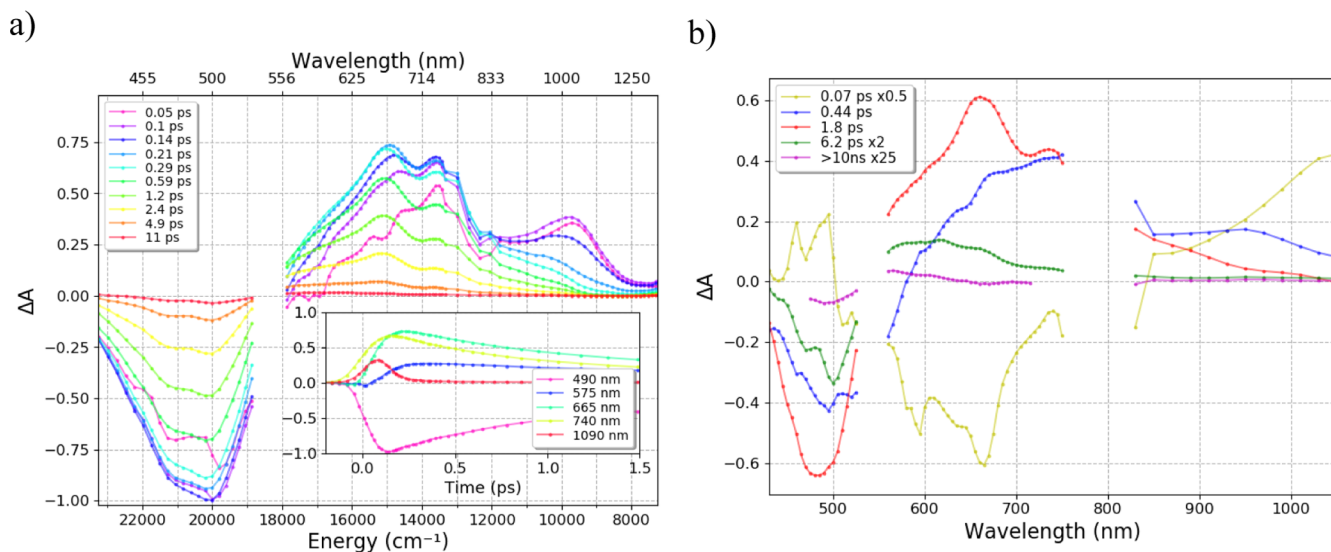


**Figure 6.** (a) Transient absorption spectra between 0.05 and 11 ps for C-tagged OCP excited at 540 nm (0.8 μJ). (b) DAS obtained from the global fit of transient absorption data. All data sets were normalized to  $-1$  at bleaching extremum (in both spectral and temporal dimensions, multiply by 0.095 to get original signal). Inset shows the evolution of the signal in 1.5 ps time window.



severely increases the negative contribution caused by photoproducts (>10 ns, DAS), which is a mixture of  $P_1$  and radical cation.

### Influence of Tagging on OCP Photophysics

The above results point to simpler photoinduced dynamics upon 540 nm excitation (no  $S^{\sim}$ ) than 470 nm excitation. Therefore, to study the influence of the His tag, only 540 nm excitation experiments at low energy (0.8  $\mu$ J) were performed. Transient spectra for C-tagged OCP-ECN after 540 nm excitation are shown in Figure 6 with DAS (four exponential components; representative kinetic traces with their fits and residuals are shown in Figure S13). The comparison with N-tagged transient spectra (Figure 2b) shows an increase in the initial absorbance at 740 nm together with a decrease in that at 663 nm (0.2 ps time delay, Figure 6a). Moreover, if one compares the transient spectra at specific time delays after 0.5 ps or the raw kinetic profiles of C-tagged versus N-tagged OCP (Figure S18), it appears that excited states decay significantly faster in C-tagged OCP. This observation is confirmed by the extraction of DAS (see Table 1). Examination of the DAS (Figure 6b) furthermore suggests that C-tagged OCP is characterized by (i) a higher contribution at 740 nm in the  $S_1$  state, (ii) a different spectral signature of the  $S^*$  state, with a smaller peak at 655 nm, and (iii) a lower positive signal of  $P_1$  (Figure S17). Nevertheless, the ratios between intermediate states are quite similar for N-tagged and C-tagged OCP. Despite these differences, the  $P_1$  formation quantum yield (Table 1) seems to be roughly similar for both N-tagged and C-tagged OCP and at worst slightly higher for C-tagged OCP. The lower contribution of  $P_1$  absorbance at 490 nm (Figure S17) can explain the slight increase in GSB amplitude and thus formation quantum yield for C-tagged OCP.

## DISCUSSION

In the present paper, we undertook a detailed photophysical study on ECN-functionalized *Synechocystis* PCC 6803 OCP with an aim to investigate its effect on photoinduced excited-state dynamics and overall activation yield of (i) excitation at either 470 nm or 540 nm, (ii) His-tagging at the N- (N-tagged) or C- (C-tagged) terminus, and (iii) excitation power. Our results show that all three factors largely influence OCP excited-state dynamics and/or photoactivation yield. Our data also question whether or not the hypothesis that  $S^*$  is the precursor of  $P_1$  (and therefore  $OCP^R$ ) is correct. Indeed, we offer demonstration that an additional excited state exists upon excitation at 470 nm and that a radical cation forms upon excitation at high energies—two points that were largely overlooked in the first study which proposed a link between  $S^*$  and  $P_1$ .<sup>9</sup> The present work should thus allow a finer understanding of OCP-embedded keto-carotenoid excited-state dynamics and may thereby open avenues toward the generation of more efficient OCP.

The most unexpected finding was that his-tagging at the N- or C- terminus influences the photoactivation speed and excited-state dynamics. Proteins are nowadays often expressed recombinantly, with N- or C-terminal extensions that facilitate their purification by affinity chromatography, and OCP is no exception. In nearly all recent studies, a His-tag was accordingly added at the N- or C-terminus, aiding purification, and avoiding degradation of the protein.<sup>1,8</sup> It should be noted that in the case of OCP, both the N-terminal and C-terminal helices appose on the same face of the CTD  $\beta$ -sheet, which

serves as the regulatory domain (Scheme 1b). Here, we show that the location of the His-tag affects (i) the photoactivation speed, as derived from initial slopes of  $OCP^R$  formation (monitored using  $\Delta A$  at 550 nm) upon continuous irradiation (slower for C-tag, Figure 1c) and (ii) the lifetime of excited states (shorter for C-tag). The population ratio between ps-lived excited states and the  $P_1$  yield is yet unaffected by the change in the position of the six-histidine tag (Table 1). It is unclear how the presence of the latter alters the lifetime and spectral signature of the excited states; however, the most likely hypothesis seems to be that these are affected by different ground-state populations of dark-adapted OCP, which each leads to different spectral signatures (notably for  $S^*$ ) and lifetimes of excited states. Regardless, the most important information is probably that the presence of the tag does not influence the  $P_1$  formation quantum yield (Table 1). Therefore, in line with our results about the influence of the carotenoid (ECN, canthaxanthin) on the photoactivation quantum yield of *Synechocystis*  $OCP^R$ ,<sup>39</sup> we attribute the effect of the tag on the photoactivation speed to molecular events occurring on the nano- and millisecond time scales, that is, related to carotenoid translocation and/or domain separation ( $P_1$  to  $OCP^R$ , Scheme 1a).<sup>10,11</sup> Studies are ongoing to better confirm this hypothesis by determining the influence of his-tagging and its location on the outcome of nanosecond flash photolysis experiments.

Because his-tagging slightly modifies the ultrafast dynamics of the OCP, comparison with earlier studies is only valid if the investigated proteins were tagged at the same location and ideally with the same tag. Ours results can thus be compared to those obtained by Konold *et al.*<sup>9</sup> who studied exactly the same N-tagged OCP-ECN (identical expression in *E. coli* and purification procedure, see materials and methods section) with 475 nm excitation and were the first to characterize and link the  $S^*$  and  $P_1$  states of OCP. To fit their excited-state transient spectra, they employed a three time constant multiexponential model accounting for three ps-lived excited-state species, *viz.*  $S_1$ , ICT, and  $S^*$ . Analogous analysis of the data set obtained upon 470 nm excitation provides similar results, including a species characterized by a DAS with a maximum at 570 nm and a time constant close to 29 ps (Figure S15). This species was assigned to  $S^*$  by Konold *et al.* (24 ps in the article<sup>9</sup>). However, these results cannot be easily compared with those we obtained upon 540 nm excitation, where  $S^*$  is characterized by a DAS peaking at 655 nm and a time constant of 7 ps. In contrast, a recent publication from Yaroshevich *et al.*<sup>13</sup> reports an  $S^*$  lifetime of 5.13 ps, in a reasonable agreement with a 7 ps lifetime derived from our data collected upon 540 nm excitation. The use of an additional time constant (extra  $S^{\sim}$  component) to fit data collected upon 470 nm excitation results in an  $S^*$  signature that is nearly identical to that obtained after 540 nm excitation (maximum of DAS at 655 nm and lifetime of about 7 ps, Figure S15). The  $S^{\sim}$  state is characterized by a DAS peaking at 570 nm and a decay time around 80 ps (Figure 5a). While accounting for only 1% of the excited-state signal upon excitation at 470 nm (Tables 1 and S1), the addition of  $S^{\sim}$  to the fitting scheme leads to a higher consistency of determined DAS and time constants for the 470 and 540 nm data sets (Figure S15).

The nature and origin of the extra  $S^{\sim}$  species is not straightforward to understand.  $S^{\sim}$  lives longer than the usually observed excited states (slightly shorter than 10 ps) and it is

absent upon 540 nm excitation. A similar state denoted as  $S^{\ddagger}$  has been observed in  $\beta$ -carotene, which is characterized by the presence of a 65 ps-lived component located at the high energy edge of ESA. The  $S^{\ddagger}$  state was found to not form upon excitation at the red edge of a  $\beta$ -carotene stationary absorption spectrum, which makes it similar to  $S^{\sim}$ .<sup>40</sup> The origin of this state was clarified in a later study where it was shown that this component disappears after extensive sample purification.<sup>41</sup> It was concluded that it must originate from minor impurities of blue-absorbing shorter chain carotenoids. Because our data clearly show that the 80 ps component does not lead to the formation of  $P_1$ , we believe that  $S^{\sim}$  in OCP is likely associated with traces of a non-photoactive carotenoid in OCP. Indeed, it was observed that ECN-OCPs produced in *E. coli* contains 1–2% of an unknown carotenoid of MW 548 and in rare cases also traces of  $\beta$ -carotene.<sup>30</sup> These OCP binding different carotenoids cannot be separated during the purification.

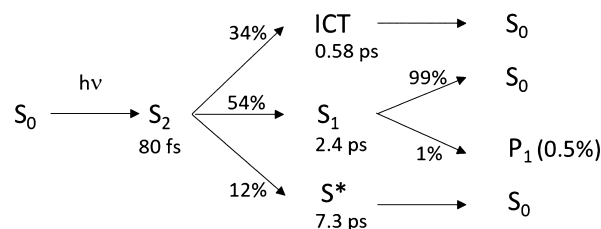
We also addressed the identity of the precursor of  $P_1$  and the interplay between the  $S^*$ , ICT, and  $S_1$  excited states. A comparison of the formation quantum yields of ICT and  $S^*$  for 470 and 540 nm excitations shows an anti-correlation (Table 1), suggesting that paths leading to these states compete. Most recently,  $S^*$  was assigned to a distorted carotenoid geometry and proposed to precede  $P_1$ .<sup>9</sup> We found using N-tagged OCP that more  $S^*$  is produced upon excitation at 470 nm than at 540 nm, despite the  $P_1$  formation quantum yield being the same value of about 0.5% at both excitation wavelengths (Table 1). Surely, the error on  $P_1$  formation quantum yield is large due its low value. Experiments aimed at exploring excitation power dependency showed that 470 nm excitation could involve additional long-lived photoproducts ( $S^{\sim}$  and radical). Hence, it is difficult to determine the quantum yield of  $P_1$  upon 470 nm excitation with high precision. It can also explain the difference with Konold *et al.* who reported a value of 1.5%.<sup>9</sup> Furthermore our value (0.5%) is consistent with the OCP<sup>R</sup> formation quantum yield estimated by Maksimov *et al.* to be about 0.2% at 200 ns using nanosecond flash photolysis studies.<sup>12</sup> Indeed Konold *et al.* showed that at 200 ns only 40% of the population of  $P_1$  remained, that is,  $P_1$  yield should be about 0.5%.<sup>9</sup> In addition, as photoactivation with continuous irradiation at either 470 or 528 nm yields the same initial slopes, we posit that the absorbance at 490 nm provides a correct estimation for the  $P_1$  formation quantum yield (Table 1). Considering that the  $S^*$  and ICT states have different yields (Table 1) at both excitation wavelengths, our data thus do not support that  $S^*$  is the main precursor of  $P_1$ . Rather, they suggest that  $S_1$  is the most probable  $P_1$  precursor with a formation quantum yield, which is similar for blue and green excitation (Table 1).

## CONCLUSIONS

In this work, the effects of excitation energy and wavelength on OCP photoactivation and excited-state dynamics were investigated in detail, as well as that of his-tagging at the N- and C-termini. Covering the NIR range (800–1400 nm) in addition to the visible spectrum, we were able to uncover the existence of a carotenoid cation radical, characterized by positive absorbance bands at 960 nm and 700 nm, and whose formation also contributes to the negative depopulation band of OCP<sup>O</sup>. This radical cation is the dominant photoproduct at 1 ns for energies exceeding the linear photoexcitation range, calling for a careful consideration of excitation energies in future transient spectroscopy studies on OCP. Excitation at

540 nm compared to 470 nm is better suited to reduce the formation of this off-pathway radical species, as a three-photon regime requires a much higher photon density in the pump pulse. This finding is of importance for the determination of the  $P_1$  formation quantum yield using the OCP<sup>O</sup> depopulation band. The formation quantum yield of  $P_1$  is close to 0.5% when the excitation power is low enough to avoid the formation of the cation radical (0.3 mJ/cm<sup>2</sup> or less for  $\lambda_{\text{exc}} = 470$  nm, 0.6 mJ/cm<sup>2</sup> or less for  $\lambda_{\text{exc}} = 540$  nm, Figures S5 and S6), consistent with previous estimates from nanosecond flash photolysis studies.<sup>12</sup> Another important result regarding 470 nm excitation is the existence of a previously unnoticed  $S^{\sim}$  species ( $\approx 80$  ps lifetime), which does not form upon excitation at 540 nm and display similar spectral features as  $P_1$ . Most likely, this  $S^{\sim}$  species originates from the presence of an unknown carotenoid in the *E. coli* cells that is not completely transformed into ECN or a secondary product that also binds OCP and cannot be removed by purifications.<sup>30</sup> Accounting for this additional species observed upon 470 nm excitation, global fitting of the data sets for the two excitation wavelengths gives similar DAS and lifetime for ICT/ $S_1$ / $S^*$  regardless of the excitation wavelength (470 vs 540 nm). Our analysis shows that the  $S^*$  lifetime is about 7 ps for 470 nm and 540 nm excitations. Because the  $S^{\sim}$  component most likely originates from a chromophore not involved in the photoactivation of OCP, modeling the dynamics using data obtained with green excitation is more relevant for the photodynamics of OCP, particularly because photoactivation experiments using continuous irradiation do not show dependence on the excitation wavelength. An important result is that the formation quantum yield for  $S^*$  and ICT differs for both excitations (Table 1), while the  $P_1$  and  $S_1$  formation quantum yield do not change. This strongly supports the hypothesis that  $S_1$ , but not  $S^*$ , is the main precursor of  $P_1$ . We thus suggest a new path for the picosecond photodynamics, leading to the  $P_1$ —photoactivation of OCP (from *Synechocystis* N-tagged with ECN), using results upon 540 nm excitation, and assuming parallel formation and decay of picosecond states (ICT,  $S_1$ , and  $S^*$ ) with yields estimated from an OCP<sup>O</sup> depopulation band (Scheme 2, Table 1).

**Scheme 2. Picosecond Photodynamics of *Synechocystis* N-Tagged ECN-OCP upon 540 nm Excitation (Yields Are Estimated from GSB Recovery of OCP<sup>O</sup> at 490 nm and  $P_1$  Represents Overall Formation Yield from  $S_2$ , Table 1)**



Finally, the comparison of ps dynamics in C-tagged *versus* N-tagged OCP revealed significant differences in the DAS and formation quantum yields of  $S^*$ , and an overall faster relaxation of excited states in C-tagged OCP. Also, the photoactivation speed observed under continuous irradiation was found to differ significantly. However, the  $P_1$  yield was unchanged. Hence, similar to our results of the influence of carotenoid (ECN, canthaxanthine) on the photoactivation quantum yield

of *Synechocystis* OCP<sup>R</sup>,<sup>39</sup> we propose that the tagging of OCP influences molecular events occurring past Ins, that is, carotenoid translocation and/or structural changes (Scheme 1a). Further studies conducted on the nanosecond-millisecond range are ongoing to verify this hypothesis.

## ■ ASSOCIATED CONTENT

### SI Supporting Information

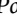
The Supporting Information is available free of charge at <https://pubs.acs.org/doi/10.1021/jacsau.1c00472>.


“Normal” and “red-shifted” sub-populations existing in the dark-adapted state, pump pulse excitation, time resolved spectra at high excitation energy, analysis of kinetics traces, and comparison of P<sub>1</sub> spectra upon different excitation *versus* His-tag and evaluation of error using bootstrapping method (PDF)

## ■ AUTHOR INFORMATION

### Corresponding Authors

**Diana Kirilovsky** – Université Paris-Saclay, CEA, CNRS, Institute for Integrative Biology of the Cell (I2BC), Gif-sur-Yvette 91198, France; Email: [Diana.KIRILOVSKY@cea.fr](mailto:Diana.KIRILOVSKY@cea.fr)

**Gotard Burdzinski** – Quantum Electronics Laboratory, Faculty of Physics, Adam Mickiewicz University in Poznań, Poznan 61-614, Poland;  [orcid.org/0000-0002-2947-1602](https://orcid.org/0000-0002-2947-1602); Email: [gotardb@amu.edu.pl](mailto:gotardb@amu.edu.pl)


**Michel Sliwa** – Univ. Lille, CNRS, UMR 8516, LASIRE, Laboratoire de Spectroscopie pour les Interactions, la Réactivité et l'Environnement, Lille S9000, France;  [orcid.org/0000-0002-5073-8180](https://orcid.org/0000-0002-5073-8180); Email: [michel.sliwa@univ-lille.fr](mailto:michel.sliwa@univ-lille.fr)

### Authors

**Stanisław Niziński** – Quantum Electronics Laboratory, Faculty of Physics, Adam Mickiewicz University in Poznań, Poznan 61-614, Poland; Univ. Lille, CNRS, UMR 8516, LASIRE, Laboratoire de Spectroscopie pour les Interactions, la Réactivité et l'Environnement, Lille S9000, France

**Adjèle Wilson** – Université Paris-Saclay, CEA, CNRS, Institute for Integrative Biology of the Cell (I2BC), Gif-sur-Yvette 91198, France

**Lucas M. Uriarte** – Univ. Lille, CNRS, UMR 8516, LASIRE, Laboratoire de Spectroscopie pour les Interactions, la Réactivité et l'Environnement, Lille S9000, France

**Cyril Ruckebusch** – Univ. Lille, CNRS, UMR 8516, LASIRE, Laboratoire de Spectroscopie pour les Interactions, la Réactivité et l'Environnement, Lille S9000, France;  [orcid.org/0000-0001-8120-4133](https://orcid.org/0000-0001-8120-4133)

**Elena A. Andreeva** – Univ. Grenoble Alpes, CEA, CNRS, Institut de Biologie Structurale, Grenoble 38000, France; Max-Planck-Institut für Medizinische Forschung, Heidelberg 69120, Germany

**Ilme Schlichting** – Max-Planck-Institut für Medizinische Forschung, Heidelberg 69120, Germany

**Jacques-Philippe Colletier** – Univ. Grenoble Alpes, CEA, CNRS, Institut de Biologie Structurale, Grenoble 38000, France

Complete contact information is available at: <https://pubs.acs.org/doi/10.1021/jacsau.1c00472>

## Notes

The authors declare no competing financial interest.

## ■ ACKNOWLEDGMENTS

This work was performed with the financial support from the Polish National Science Centre (NCN), project 2018/31/N/ST4/03983, and the French National Research Agency (grant ANR-18-CE11-0005 to M.S., D.K., I.S., and J.P.C.).

## ■ REFERENCES

- (1) Holt, T. K.; Krogmann, D. W. A carotenoid-protein from cyanobacteria. *Biochim. Biophys. Acta* **1981**, *637*, 408–414.
- (2) Kirilovsky, D.; Kerfeld, C. A. Cyanobacterial photoprotection by the orange carotenoid protein. *Nat. Plants* **2016**, *2*, 16180.
- (3) Sluchanko, N. N.; Slonimskiy, Y. B.; Maksimov, E. G. Features of protein–protein interactions in the cyanobacterial photoprotection mechanism. *Biochemistry* **2017**, *82*, 1592–1614.
- (4) Muzzopappa, F.; Kirilovsky, D. Changing color for photoprotection: The Orange Carotenoid Protein. *Trends Plant Sci.* **2020**, *25*, 92–104.
- (5) Wilson, A.; Punginelli, C.; Gall, A.; Bonetti, C.; Alexandre, M.; Routaboul, J.-M.; Kerfeld, C. A.; van Grondelle, R.; Robert, B.; Kennis, J. T. M.; Kirilovsky, D. A photoactive carotenoid protein acting as light intensity sensor. *Proc. Natl. Acad. Sci. U.S.A.* **2008**, *105*, 12075–12080.
- (6) Wilson, A.; Gwizdala, M.; Mezzetti, A.; Alexandre, M.; Kerfeld, C. A.; Kirilovsky, D. The essential role of the N-terminal domain of the orange carotenoid protein in cyanobacterial photoprotection: importance of a positive charge for phycobilisome binding. *Plant Cell* **2012**, *24*, 1972–1983.
- (7) Leverenz, R. L.; Jallet, D.; Li, M.-D.; Mathies, R. A.; Kirilovsky, D.; Kerfeld, C. A. Structural and Functional Modularity of the Orange Carotenoid Protein: Distinct Roles for the N- and C-Terminal Domains in Cyanobacterial Photoprotection. *Plant Cell* **2014**, *26*, 426–437.
- (8) Kerfeld, C. A.; Sawaya, M. R.; Brahmandam, V.; Cascio, D.; Ho, K. K.; Trevithick-Sutton, C. C.; Krogmann, D. W.; Yeates, T. O. The crystal structure of a cyanobacterial water-soluble carotenoid binding protein. *Structure* **2003**, *11*, 55–65.
- (9) Konold, P. E.; van Stokkum, I. H. M.; Muzzopappa, F.; Wilson, A.; Groot, M.-L.; Kirilovsky, D.; Kennis, J. T. M. Photoactivation mechanism, timing of protein secondary structure dynamics and carotenoid translocation in the Orange Carotenoid Protein. *J. Am. Chem. Soc.* **2019**, *141*, 520–530.
- (10) Leverenz, R. L.; Sutter, M.; Wilson, A.; Gupta, S.; Thurotte, A.; Bourcier de Carbon, C.; Petzold, C. J.; Ralston, C.; Perreau, F.; Kirilovsky, D.; Kerfeld, C. A. A 12 Å carotenoid translocation in a photoswitch associated with cyanobacterial photoprotection. *Science* **2015**, *348*, 1463–1466.
- (11) Maksimov, E. G.; Protasova, E. A.; Tsoraev, G. V.; Yaroshevich, I. A.; Maydykovskiy, A. I.; Shirshin, E. A.; Gostev, T. S.; Jelzow, A.; Moldenhauer, M.; Slonimskiy, Y. B.; Sluchanko, N. N.; Friedrich, T. Probing of carotenoid-tryptophan hydrogen bonding dynamics in the single-tryptophan photoactive Orange Carotenoid Protein. *Sci. Rep.* **2020**, *10*, 11729.
- (12) Maksimov, E. G.; Sluchanko, N. N.; Slonimskiy, Y. B.; Slutskaya, E. A.; Stepanov, A. V.; Argentova-Stevens, A. M.; Shirshin, E. A.; Tsoraev, G. V.; Klementiev, K. E.; Slatinskaya, O. V.; Lukashev, E. P.; Friedrich, T.; Paschenko, V. Z.; Rubin, A. B. The photocycle of orange carotenoid protein conceals distinct intermediates and asynchronous changes in the carotenoid and protein components. *Sci. Rep.* **2017**, *7*, 15548.
- (13) Yaroshevich, I. A.; Maksimov, E. G.; Sluchanko, N. N.; Zlenko, D. V.; Stepanov, A. V.; Slutskaya, E. A.; Slonimskiy, Y. B.; Botnarevskii, V. S.; Remeeva, A.; Gushchin, I.; Kovalev, K.; Gordeliy, V. I.; Shelaev, I. V.; Gostev, F. E.; Khakhulin, D.; Poddubnyy, V. V.; Gostev, T. S.; Cherepanov, D. A.; Polívka, T.; Kloz, M.; Friedrich, T.; Paschenko, V. Z.; Nadtochenko, V. A.; Rubin,



- A. B.; Kirpichnikov, M. P. Role of hydrogen bond alternation and charge transfer states in photoactivation of the Orange Carotenoid Protein. *Commun. Biol.* **2021**, *4*, 539.
- (14) Šlouf, V.; Kuznetsova, V.; Fuciman, M.; de Carbon, C. B.; Wilson, A.; Kirilovsky, D.; Polívka, T. Ultrafast spectroscopy tracks carotenoid configurations in the orange and red carotenoid proteins from cyanobacteria. *Photosynth. Res.* **2017**, *131*, 105–117.
- (15) Berera, R.; Gwizdala, M.; van Stokkum, I. H. M.; Kirilovsky, D.; van Grondelle, R. Excited states of the inactive and active forms of the Orange Carotenoid Protein. *J. Phys. Chem. B* **2013**, *117*, 9121–9128.
- (16) Berera, R.; van Stokkum, I. H. M.; Gwizdala, M.; Wilson, A.; Kirilovsky, D.; van Grondelle, R. The photophysics of the orange carotenoid protein, a light-powered molecular switch. *J. Phys. Chem. B* **2012**, *116*, 2568–2574.
- (17) Polívka, T.; Chábera, P.; Kerfeld, C. A. Carotenoid–protein interaction alters the S1 energy of hydroxyechinenone in the Orange Carotenoid Protein. *Biochim. Biophys. Acta* **2013**, *1827*, 248–254.
- (18) Chábera, P.; Durchan, M.; Shih, P. M.; Kerfeld, C. A.; Polívka, T. Excited-state properties of the 16kDa red carotenoid protein from *Arthrospira maxima*. *Biochim. Biophys. Acta* **2011**, *1807*, 30–35.
- (19) Andersson, P. O.; Gillbro, T. Photophysics and dynamics of the lowest excited singlet state in long substituted polyenes with implications to the very long-chain limit. *J. Chem. Phys.* **1995**, *103*, 2509–2519.
- (20) Gradinaru, C. C.; Kennis, J. T. M.; Papagiannakis, E.; van Stokkum, I. H. M.; Cogdell, R. J.; Fleming, G. R.; Niederman, R. A.; van Grondelle, R. An unusual pathway of excitation energy deactivation in carotenoids: Singlet-to-triplet conversion on an ultrafast timescale in a photosynthetic antenna. *Proc. Natl. Acad. Sci. U.S.A.* **2001**, *98*, 2364–2369.
- (21) Lenzer, T.; Ehlers, F.; Scholz, M.; Oswald, R.; Oum, K. Assignment of carotene S\* state features to the vibrationally hot ground electronic state. *Phys. Chem. Chem. Phys.* **2010**, *12*, 8832–8839.
- (22) Balevičius, V.; Abramavicius, D.; Polívka, T.; Galestian Pour, A.; Hauer, J. A unified picture of S\* in carotenoids. *J. Phys. Chem. Lett.* **2016**, *7*, 3347–3352.
- (23) Khan, T.; Dominguez-Martin, M. A.; Šimová, I.; Fuciman, M.; Kerfeld, C. A.; Polívka, T. Excited-state properties of canthaxanthin in cyanobacterial carotenoid-binding proteins HCP2 and HCP3. *J. Phys. Chem. B* **2020**, *124*, 4896–4905.
- (24) Kuznetsova, V.; Dominguez-Martin, M. A.; Bao, H.; Gupta, S.; Sutter, M.; Kloz, M.; Rebarz, M.; Přeček, M.; Chen, Y.; Petzold, C. J.; Ralston, C. Y.; Kerfeld, C. A.; Polívka, T. Comparative ultrafast spectroscopy and structural analysis of OCP1 and OCP2 from *Tolypothrix*. *Biochim. Biophys. Acta* **2020**, *1861*, 148120.
- (25) Lincoln, C. N.; Fitzpatrick, A. E.; Thor, J. J. v. Photoisomerisation quantum yield and non-linear cross-sections with femtosecond excitation of the photoactive yellow protein. *Phys. Chem. Chem. Phys.* **2012**, *14*, 15752–15764.
- (26) van Stokkum, I. H. N.; Larsen, D. S.; Grondelle, R. Global and target analysis of time-resolved spectra. *Biochim. Biophys. Acta, Bioenerg.* **2004**, *1657*, 82–104.
- (27) Khan, T.; Kuznetsova, V.; Dominguez-Martin, M. A.; Kerfeld, C. A.; Polívka, T. UV excitation of carotenoid binding proteins OCP and HCP: excited-state dynamics and product formation. *ChemPhotoChem* **2022**, *6*, No. e202100194.
- (28) Polívka, T.; Kerfeld, C. A.; Pascher, T.; Sundström, V. Spectroscopic Properties of the Carotenoid 3'-Hydroxyechinenone in the Orange Carotenoid Protein from the Cyanobacterium *Arthrospira maxima*. *Biochemistry* **2005**, *44*, 3994–4003.
- (29) Kish, E.; Pinto, M. M. M.; Kirilovsky, D.; Spezia, R.; Robert, B. Echinenone vibrational properties: From solvents to the orange carotenoid protein. *Biochim. Biophys. Acta* **2015**, *1847*, 1044–1054.
- (30) de Carbon, C. B.; Thurotte, A.; Wilson, A.; Perreau, F.; Kirilovsky, D. Biosynthesis of soluble carotenoid holoproteins in *Escherichia coli*. *Sci. Rep.* **2015**, *5*, 9085.
- (31) Gwizdala, M.; Wilson, A.; Kirilovsky, D. In vitro reconstitution of the cyanobacterial photoprotective mechanism mediated by the Orange Carotenoid Protein in *Synechocystis* PCC 6803. *Plant Cell* **2011**, *23*, 2631–2643.
- (32) Brazevic, S.; Nizinski, S.; Sliwa, M.; Abe, J.; Rode, M. F.; Burdzinski, G. Control of the photo-isomerization mechanism in 3H-naphthopyrans to prevent formation of unwanted long-lived photo-products. *Int. J. Mol. Sci.* **2020**, *21*, 7825.
- (33) Wendel, M.; Nizinski, S.; Tuwalska, D.; Starzak, K.; Szot, D.; Prukala, D.; Sikorski, M.; Wybraniec, S.; Burdzinski, G. Time-resolved spectroscopy of the singlet excited state of betanin in aqueous and alcoholic solutions. *Phys. Chem. Chem. Phys.* **2015**, *17*, 18152–18158.
- (34) Uriarte, L. M.; Niziński, S.; Labarrière, L. *Ultraparfyt a python package for time resolved data*; Zenodo, 2021.
- (35) Snellenburg, J. J.; Laptinok, S. P.; Seger, R.; Mullen, K. M.; van Stokkum, I. H. M. Glotaran: A Java-based graphical user interface for the R package TMAP. *J. Stat. Softw.* **2012**, *49*, 1–22.
- (36) Pigni, N. B.; Clark, K. L.; Beck, W. F.; Gascón, J. A. Spectral signatures of canthaxanthin translocation in the Orange Carotenoid Protein. *J. Phys. Chem. B* **2020**, *124*, 11387–11395.
- (37) Jeevarajan, J. A.; Wei, C. C.; Jeevarajan, A. S.; Kispert, L. D. Optical absorption spectra of dications of carotenoids. *J. Phys. Chem.* **1996**, *100*, 5637–5641.
- (38) Gao, G.; Wei, C. C.; Jeevarajan, A. S.; Kispert, L. D. Geometrical isomerization of carotenoids mediated by cation radical/dication formation. *J. Phys. Chem.* **1996**, *100*, 5362–5366.
- (39) Wilson, A.; Andreeva, E. A.; Nizinski, S.; Talbot, L.; Hartmann, E.; Schlichting, I.; Burdzinski, G.; Sliwa, M.; Kirilovsky, D.; Colletier, J.-P. Structure-function-dynamics relationships in the peculiar *Planktothrix* PCC7805 OCP1: impact of his-tagging and carotenoid type. *Biorxiv* **2022**, DOI: 10.1101/2022.01.04.474796.
- (40) Larsen, D. S.; Papagiannakis, E.; van Stokkum, I. H. M.; Vengris, M.; Kennis, J. T. M.; Grondelle, R. Excited state dynamics of  $\beta$ -carotene explored with dispersed multi-pulse transient absorption. *Chem. Phys. Lett.* **2003**, *381*, 733–742.
- (41) Ostroumov, E. E.; Reus, M. G. M. M.; Holzwarth, A. R.; Holzwarth, A. R. On the nature of the “Dark S\*” excited state of  $\beta$ -Carotene. *J. Phys. Chem. A* **2011**, *115*, 3698–3712.